Langmuir

Article

pubs.acs.org/Langmuir

Bidentate Surface Structures of Glycylglycine on Si(111)7×7 by High-Resolution Scanning Tunneling Microscopy: Site-Specific Adsorption via N−H and O−H or Double N−H Dissociation

A. Chatterjee, L. Zhang, and K. T. Leung*

WATLab and Department of Chemistry, University of Waterloo, Waterloo, Ontario N2L 3G1, Canada

ABSTRACT: The early adsorption stage of glycylglycine on Si(111)7×7 surface has been studied by scanning tunneling microscopy (STM). Filled-state imaging shows that glycylglycine adsorbs dissociatively in a bidentate fashion on two adjacent Si adatoms across a dimer wall or an adatom−restatom pair, with the dissociated H atoms on neighboring restatoms. The present STM result validates our hypothesis that both bidentate configurations involving N−H and O−H dissociation and double N−H dissociation are equally probable. Our STM results further show that the relative surface concentrations of the five bidentate configurations follow a specific ordering. This suggests that N−H dissociation at a center adatom site would likely be followed by N−H dissociation at an adjacent restatom, while N−H dissociation at a corner adatom site would be succeeded by O−H dissociation at an adatom across the dimer wall. Evidently, the strong bidentate interactions also inhibit surface diffusion of the adsorbed glycylglycine fragment, and the adsorption apparently follows random sequential adsorption statistics. The random nature of adsorption is also supported by the similar relative occupancies of the center adatom and corner adatom sites, indicating that the relative reactivities of these adatom sites do not play a significant role. Our DFT computational study shows that all three bidentate (Si−)$NHCH_2CONHCH_2COO$(−Si) adatom−adatom configurations (center−center, corner−corner, center−corner) have similar adsorption energies for a double adatom−adatom pair across the dimer wall, while the (Si−)$NHCH_2CON$(−Si)CH_2COOH bidentate adatom−restatom configuration is energetically favorable. The free −CONH− and −COOH groups remaining on the respective bidentate adstructures could facilitate adsorption of the second adlayer through the formation of hydrogen bonding.

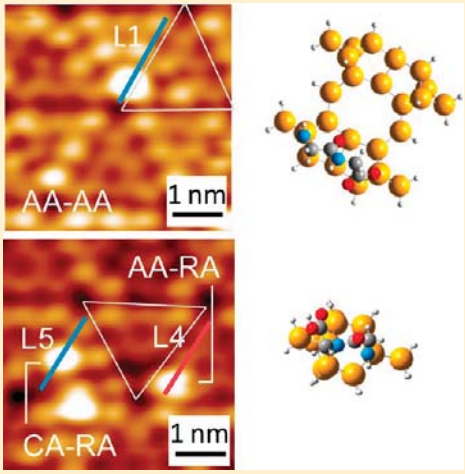

1. INTRODUCTION

Organic functionalization of semiconductor surfaces has provided the impetus of incorporating biological molecules into existing electronic components for novel bioelectronic devices, biosensors, and nanotechnology applications.[1−5] Among the semiconductor materials, silicon continues to attract the most attention because Si single-crystal surfaces provide the singularly most important platform for fabricating microelectronic devices, often under ultrahigh vacuum conditions. Silicon single-crystal surfaces therefore offer the natural starting point for functional integration of biomolecules to improve performance and/or to add new functions, for example, in molecular electronics and biosensing applications.[6,7] This type of biodevice development requires a better understanding of Si surface chemistry, particularly the surface reactions with prototypical biomolecules under ultrahigh vacuum conditions.

Si(111)7×7 and Si(100)2×1 represent two of the most fundamental (and most studied) semiconductor surfaces, and they offer unique bonding sites, each with one and two directional dangling bonds (unsaturated valencies), respectively, for interactions with the approaching adsorbates. In the asymmetric buckled dimer model for the Si(100)2×1 surface, one of the dangling bonds from each of two neighboring atoms forms a strong σ bond with each other, while the remaining dangling bond combines with that of a neighboring atom to form a weak π bond, creating a Si−Si dimer.[8,9] Charge transfer from the down-atom to the up-atom of the buckled dimer leads to the formation of an electrophilic−nucleophilic pair.[9,10] This structure of nucleophilic top layer (of the up-atoms) followed by an electrophilic second layer (of the down-atoms) is in marked contrast to the case of Si(111)7×7 surface. In the dimer-adatom-stacking-fault model proposed by Takayanagi et al.,[11] the 7×7 unit cell consists of 12 adatoms (in the topmost layer), 6 restatoms (in the next layer) and 1 corner-hole-atom (in the third layer), each with a dangling bond, thereby reducing the total number of dangling bonds from 49 in the unreconstructed surface to 19 in the reconstructed surface. The adatom−restatom pair (with the adatom-to-restatom separation of 4.57 Å) provides the most important reaction site for the

Received: May 31, 2012
Revised: July 17, 2012
Published: August 17, 2012

smaller organic molecules with similar dimensions, including glycine.[12] Furthermore, the adatom is reported to have less electron occupancy than the restatom due to a small charge transfer from the adatom to the restatom, resulting in formal charges of ∼+1 for the center adatom, ∼+7/12 for the corner adatom, and ∼−1 for the restatom.[13] Consequently, the topmost layer of the Si(111)7×7 surface (with the adatoms) is more electrophilic in nature, in contrast to the nucleophilic next layer of the restatoms. Because a center adatom has two neighboring restatoms, it has even less electron occupancy and is therefore more electrophilic than the corner adatom. The difference in their electronic environments leads to different surface reactions, resulting in their selectivities toward specific organic molecules with different functional groups.[10,12]

Not surprisingly, a large number of studies has been reported on the chemistry of these two fundamental surfaces: Si(111)7×7 and Si(100)2×1, particularly on their interactions with small molecules (e.g., H_2, O_2, N_2, CO, NH_3, H_2O),[14] simple aliphatic hydrocarbons (e.g., acetylene, ethylene, butadiene) and aromatic compounds (e.g., benzene, pyrrole, pyridine, thiophene), as well as common organic molecules with a single functional group (e.g., methanol and ethanol, acetic acid, dimethylamine).[7] However, there are considerably less work on bifunctional molecules (e.g., acrylic acid,[15] allyl alcohol,[16] allyl amine,[8] ethanolamine)[17] and more complex molecules with multiple groups, for example, $-NH_2$ and −OH, −COOH and C═C. Even less studies have been reported for organic molecules with biological interest, including, for example, glycine,[18−22] glyclyglycine,[23] adenine,[24] thymine,[25] and zwitterionic assemblies such as [4-methoxy-*N*-(3-sulfonatopropyl)pyridinium].[26]

Biomolecules are generally complex in nature, and some can be considered polymers of identical units (building blocks) or of combinations of different units. For example, a peptide is a polymer of amino acids, while a DNA molecule is a polymer of four nucleobases (adenine, guanine, cytosine, and thymine) with sugar phosphate backbones. Glycylglycine (GG) is the simplest peptide consisting of two glycine residues connected by a single peptide bond. Recently, we have reported studies of the interactions of glycine with the Si(111)7×7 surface by X-ray photoelectron spectroscopy (XPS)[20] and scanning tunneling microscopy (STM),[27] along with appropriate ab initio calculations based on density functional theory (DFT). We now extend this work to the interactions of GG with the 7×7 surface by STM, using our recent XPS/DFT results[23] to provide the local bonding information as the basis to infer the intriguing site-specific chemistry. In our recent XPS/DFT study, we show that the early growth stage of GG involves either N−H and O−H dissociation or double N−H dissociation. These types of surface dissociative adsorption lead to bidentate adstructures with the formation of a N−Si and a O−Si bond or of double N−Si bonds, respectively.[23] Increasing the GG exposure on Si(111)7×7 surface leads to the introduction of a hydrogen bonded transitional adlayer, which promotes the eventual formation of a GG zwitterionic (thick) film.[23] In the present work, we investigate the early growth stage of GG on the 7×7 surface by using high resolution STM, and determine the plausible bidentate adsorption configurations on different sites. In marked contrast to glycine adsorption where hydrogen bonding plays a pivotal role,[20] the strong bidentate adstructure−substrate interactions of GG with the 7×7 surface reduce the surface diffusion, and the adsorption essentially follows random sequential statistics.

2. EXPERIMENTAL AND COMPUTATIONAL DETAILS

All the experiments were performed in a five-chamber ultrahigh vacuum system (Omicron Nanotechnology, Inc.) with a base pressure better than 3×10^{-11} mbar, described in detail elsewhere.[20] The analysis chamber was equipped with both an XPS system (consisting of the SPHERA hemispherical analyzer and a monochromatized Al Kα source) and a variable-temperature scanning probe microscope (VT-SPM) for atomic-resolution imaging. The STM images were obtained with an electrochemically etched, atomically sharp W tip, prepared by using a modified electrochemical etching procedure with a ring electrode similar to that discussed by Klein and Schwitzgebel.[28] The STM images were recorded at room temperature in a constant current mode with the feedback loop on during measurement. Single-side polished Si(111) chips (11×2 mm^2, 0.3 mm thick, n-type, As doped) with a resistivity of 5 mΩ cm (Virginia Semiconductor Inc.) were used as the substrates. The substrates were cleaned by first outgassing at ∼400 °C overnight, followed by flash annealing at ∼1200 °C several times by direct-current heating until large areas of contaminant-free 7×7 terraces were observed in the STM images. GG (>99.5% purity, Sigma-Aldrich), with a normal melting point of ∼220 °C, was deposited onto the Si substrates by thermal evaporation using a water-cooled effusion cell (designed specifically for low-temperature organic material evaporation) in a separate organic molecular beam epitaxy chamber. During GG evaporation, the temperature of the effusion cell was kept at 170 °C, with the chamber pressure rising to $3-4 \times 10^{-9}$ mbar. The molecular nature of GG vapor was verified by the presence of the parent-ion and base-ion peaks at 132 and 30 amu, respectively, in its mass spectra recorded with a quadrupole mass spectrometer before sample dosing.[29] Deposition time is used here to indicate the relative exposure of GG, while the absolute coverage of GG can be obtained directly from the corresponding STM images.

Electronic structure calculations were performed by using the GAUSSIAN 09 software.[30] Based on the dimer-adatom-stacking-fault model,[11] we employed a $Si_{16}H_{18}$ cluster to simulate the adatom−restatom pair, as described in our earlier work.[23] In addition, we also used a $Si_{26}H_{24}$ cluster to model the double adatom−adatom pair across the dimer wall of the 7×7 unit cell, with the adatom−adatom separation constrained at 6.65 Å. The equilibrium structures of GG on these clusters were optimized by using the DFT method with the B3LYP hybrid functional[31,32] and the 6-31++G(d,p) basis set. Full frequency calculations at the same level of theory were also performed to ensure the absence of any imaginary frequency and that the resulting adsorbate−substrate configurations (ASCs) correspond to global minima on the potential energy surface. The adsorption energy for an ASC was estimated by the difference between the total energy of the ASC and the sum of the total energies of a free GG molecule (in its straight-chain conformer form)[33] and the corresponding cluster.

3. RESULTS AND DISCUSSION

Figure 1 shows the high-resolution filled-state and empty-state STM images of a 15 s GG exposure on Si(111)7×7 recorded with sample bias voltages of −2 V and +2 V, respectively, and a constant tunneling current of 150 pA. Schematic diagrams depicting an unreacted unit cell (A) and a reacted unit cell (B) for the respective images are shown in Figure 1c and d. Evidently, for the unreacted unit cell A, the filled-state image clearly shows the presence of the restatoms and discerns the faulted and unfaulted halves with the former being notably brighter than the latter (Figure 1a, c). The relative levels of brightness of the faulted and unfaulted halves are also illustrated by the generally higher height profile of the adatoms along linescan L2 of the faulted half than that along L1 of the unfaulted half (Figure 1e). The height of the center adatom (CA) is found to be lower than that of the corner (*angulus* in Latin) adatoms (AA), which indicates that the local density of states (LDOS) of CA is lower than that of AA. This is consistent with the charge transfer from a CA to both of its

dx.doi.org/10.1021/la302225z | *Langmuir* 2012, 28, 12502−12508

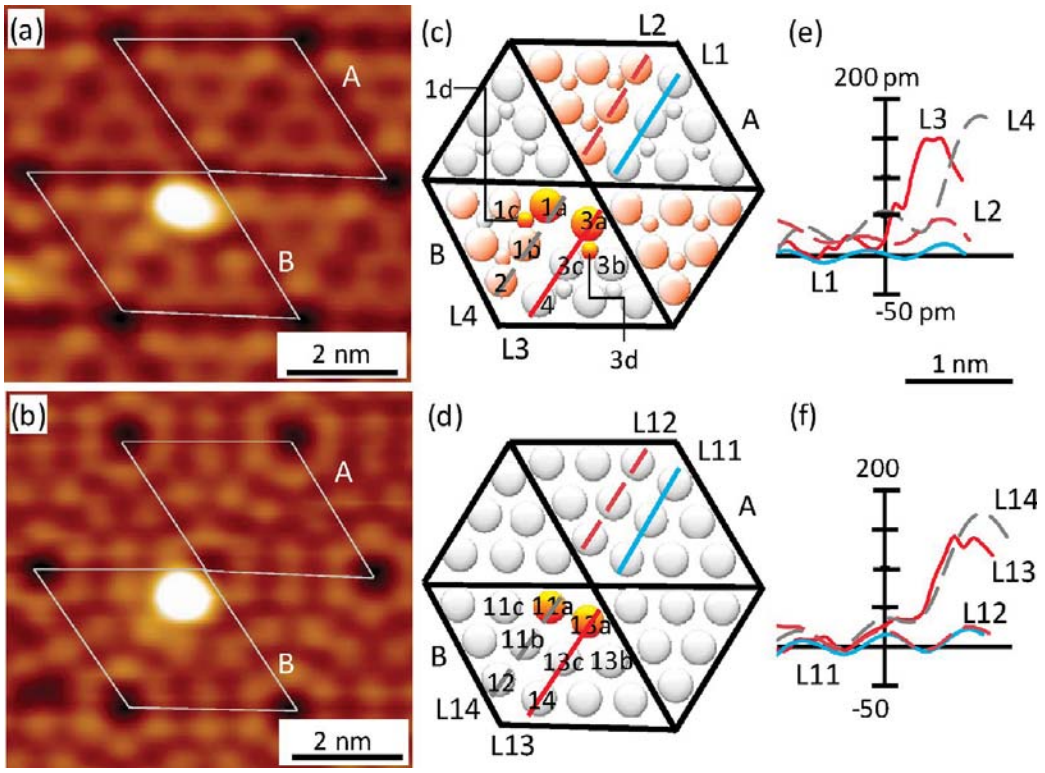

Figure 1. (a) STM filled-state image and (b) empty-state image of glyclyglycine adsorbed on a Si(111)7×7 surface obtained with a sample bias −2 V and +2 V, respectively, all at a constant tunneling current of 150 pA. (c, d) Corresponding schematic diagrams depicting (A) an unreacted and (B) a reacted 7×7 unit cells, and (e, f) height profiles along the linescans Lx (x = 1−4, 11−14) in the unfaulted half (marked by solid lines) and faulted half (marked by dashed lines). The atoms in the unfaulted and faulted half unit cells are represented by lighter and darker spheres in (c), respectively. The sites of interest are labeled by alphanumeric characters.

neighboring restatoms (RAs) being greater than the charge transfer from an AA to its only RA neighbor. On the other hand, the empty-state image for the unreacted unit cell A (Figure 1b) shows all adatoms with essentially the same brightness on both the faulted and unfaulted halves, which is also illustrated by the nearly overlapping height profiles along linescans L12 and L11, respectively (Figure 1f). As the restatoms are not visible in the empty-state images, empty-state imaging is therefore less useful for probing dissociative adsorption that involves the restatoms, as shown for glycine[34] and the present case.

For the reacted unit cell B, the filled-state STM image (Figure 1a) shows a bright protrusion covering two adatoms (AA1a, AA3a) across the dimer wall, suggesting a bidentate adsorption arrangement involving both corner adatoms (AA-AA). The absence of intensities at the expected locations of the restatoms (RA1d, RA3d) suggests the presence of H atoms dissociated from a GG molecule, following the similar observation for glycine adsorption on the 7×7 surface.[34] Furthermore, H adsorption at the restatoms also cause brightness enhancement of the adjacent adatoms (CA1b, CA1c for RA1d, and CA3b, CA3c for RA3d). This brightness enhancement is quite apparent from the higher height profile along linescan L3 (L4) at the CA3c (CA1b) position relative to that along L1 (L2) at the corresponding CA position of the unreacted unit cell (Figure 1e). Our recent XPS and DFT study of GG adsorption on Si(111)7×7 has concluded that the GG molecule undergoes N−H and O−H or double N−H dissociations to produce a bidentate adstructure. The two dissociated H atoms could land on the adjacent restatoms, causing dark depressions at the corresponding RA positions in the STM filled-state image, and terminate the Si dangling bonds with the formation of the Si−H bonds, which leads to the brighter appearance of the neighboring unreacted adatoms as a result of the charge transfer from the reacted restatom. Given that the separation of N−H to C(O)N−H in GG (3.74 Å) is too small to bridge two adatoms across the dimer wall (6.65 Å), only N−H and O−H dissociation at the two termini could be compatible with this separation. The corresponding empty-state image (Figure 1b) also shows a bright protrusion over AA11a and AA13a, which is also depicted by the more intense peaks at the respective AA locations along linescans L14 and L13 of the reacted unit cell B when compared to those along L12 and L11 of the unreacted unit cell A (Figure 1f).

In addition to the filled-state STM image shown in Figure 1, we also observe three other common patterns that correspond to other types of bidentate configurations of GG on the 7×7 surface for the other GG exposures employed in the present study. Figure 2 compares these four filled-state STM images recorded at −2 V bias voltage, along with their respective height profiles and possible ASCs (in both top and side views) obtained by DFT/6-31++G(d,p) calculations. In particular, Figure 2a1 shows another example of a bright protrusion over two corner adatoms across the dimer wall, with a separation of 6.65 Å, which corresponds to an AA-AA bidentate ASC (Figure 2c1) as in Figure 1. Similarly, Figure 2a2 shows a bright protrusion over two center adatoms across the dimer wall. The corresponding CA-CA bidentate ASC (Figure 2c2) could be

dx.doi.org/10.1021/la302225z | Langmuir 2012, 28, 12502−12508

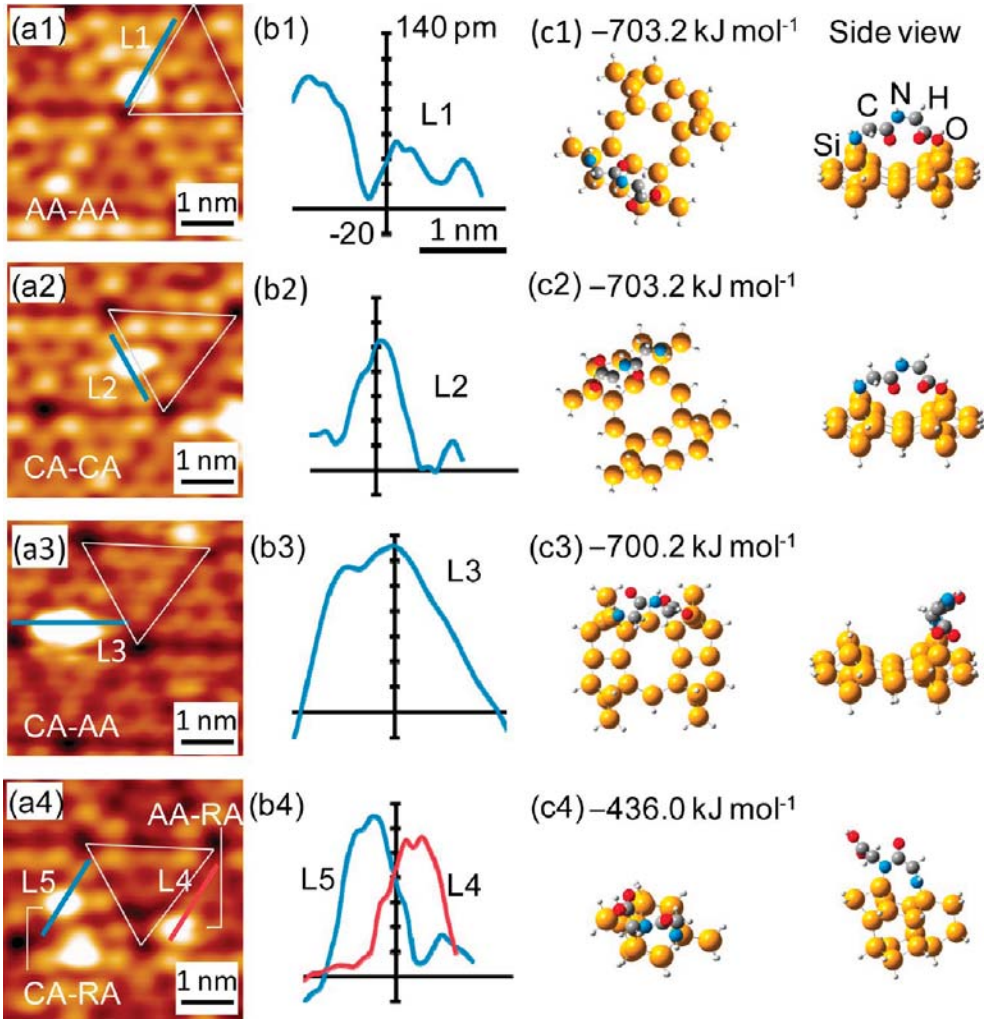

Figure 2. (a) STM filled-state images taken at a sample bias of −2 V and a tunneling current of 150 pA, (b) height profiles along the respective linescans, L1-L5, for bidentate adsorption of glycylglycine on the AA-AA, CA-CA, CA-AA and CA-RA or AA-RA sites, and the corresponding plausible equilibrium adstructures, with top (center right column) and side views (right column), and adsorption energies of glycylglycine on (c1−3) $Si_{26}H_{24}$ and (c4) $Si_{16}H_{18}$, all obtained with DFT/B3LYP/6-31G++(d,p).

approximated by the same bidentate ASC shown in Figure 2c1. The corresponding height profiles along linescans L1 and L2 show that both bidentate ASCs exhibit similar heights (100−110 pm) for the respective reacted adatoms. Furthermore, Figure 2a3 depicts a bright protrusion over a center adatom and a corner adatom on the same side of the dimer wall with a separation of 7.68 Å, which corresponds to a CA-AA bidentate ASC shown in Figure 2c3. (It should be noted that the separation between a center adatom and a corner adatom diagonally across the dimer wall is 10.14 Å). Evidently, the NH_2 to COOH separation in a straight-chain GG conformer (6.08 Å) is compatible with the adatom−adatom separations for AA-AA, CA-CA, and CA-AA bidentate configurations. Figure 2a4 shows two bright protrusions, each of which is located over an adatom−restatom pair corresponding to a CA-RA ASC with double N−H dissociations from the amine and peptide groups. The discernibly narrower widths of the height profiles along linescans L4 and L5 are consistent with the shorter CA-RA (or AA-RA) separation of 4.56 Å than the AA-AA or CA-CA and CA-AA separations. This CA-RA (or AA-RA) separation closely matches the shorter NH_2 to CONH distance in the GG molecule (3.74 Å). However, it is not possible to differentiate between the two different bidentate configurations: (XA−)-$NHCH_2CON(-RA)CH_2COOH$ and (RA−)$NHCH_2CON$-$(-XA)CH_2COOH$ (where XA = CA or AA) from our STM image (Figure 2a4). Our present STM results are in good accord with our calculations reported in our recent work.[23] In particular, the bidentate ASCs involving N−H and O−H dissociations (with adsorption energies of −703.22 kJ mol^{-1} for AA-AA or CA-CA and −700.20 kJ mol^{-1} for CA-AA) and double N−H dissociations (with an adsorption energy of −436.0 kJ mol^{-1} for CA-RA or AA-RA) are favored thermodynamically. We could also rule out the less thermodynamically stable unidentate ASCs, because of the absence of any bright protrusion correlated with only one adjacent dark depression corresponding to a single dissociated H atom in any of the STM images examined in the present work.

Figure 3 shows the filled-state STM images collected over a 50 × 50 nm^2 area for five different exposures of GG (from 15 to 40 s) on Si(111)7×7. For better illustration, we show selected 20 × 20 nm^2 areas for four of the five exposures. These images

dx.doi.org/10.1021/la302225z | Langmuir 2012, 28, 12502−12508

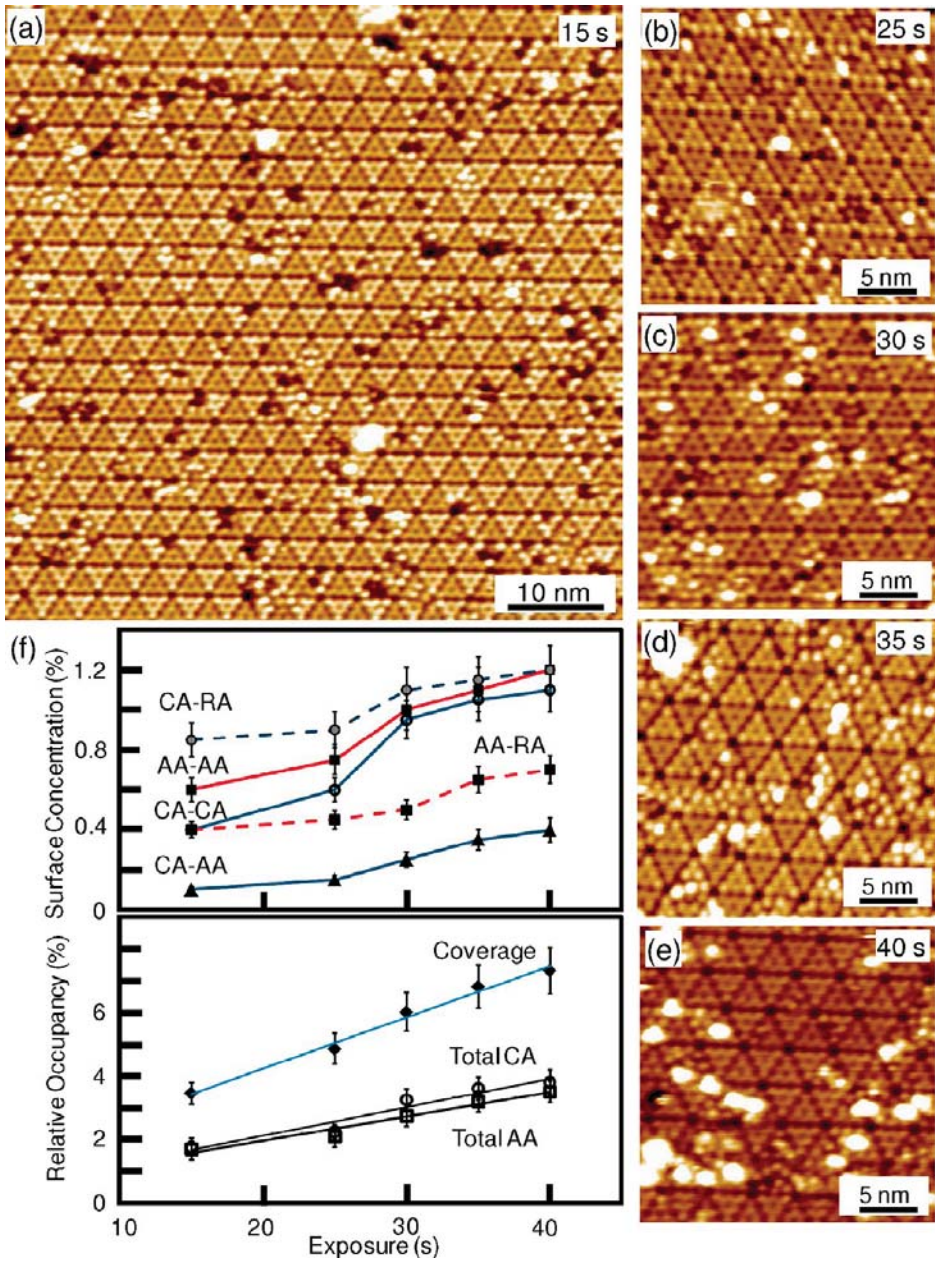

Figure 3. STM filled-state images taken at a sample bias of −2 V and a tunneling current of 150 pA after glycylglycine exposure of (a) 15 s, (b) 25 s, (c) 30 s, (d) 35 s, and (e) 40 s; and (f) the relative surface concentrations for bidentate adsorption at CA-RA, AA-AA, CA-CA, AA-RA, and CA-AA sites and the total coverage and relative occupancies for total reacted CA and AA sites.

reveal that random distributions of the five bidentate configurations described in Figure 2, with no notable spatial correlation among the bidentate configurations. Figure 3f shows the corresponding relative surface concentrations of these five bidentate configurations as a function of GG exposure. The surface concentration for a particular bidentate configuration is obtained by counting its number of occurrences, and then dividing the resulting number by the total number of available adatom sites in the full 50 × 50 nm^2 STM image. A 50 × 50 nm^2 surface area contains approximately 400 7×7 unit cells with a total of 4800 Si adatoms and 2400 restatoms. Evidently, the surface concentrations of all five bidentate configurations appear to have rather similar increasing trend with increasing exposure. At the initial adsorption stage (15 s), the relative surface concentration of CA-RA bidentate configuration is found to be the highest among all the other bidentate configurations, representing almost 37% of the total GG adsorption on the surface. This is followed by AA-AA (25%), CA-CA (17%), AA-RA (17%), and CA-AA bidentate configurations (4%). The relative surface concentrations of these bidentate configurations follow the essentially same ordering: CA-RA > AA-AA > CA-CA > AA-RA > CA-AA, with increasing exposure. Interestingly, the surface concentrations of AA-AA and CA-CA bidentate configurations appear to increase with a discernibly greater slope with respect to the exposure than the other bidentate configurations (CA-RA, AA-RA, CA-AA).

dx.doi.org/10.1021/la302225z | *Langmuir* 2012, 28, 12502−12508

Upon N−H dissociative adsorption of GG on a CA site, the adstructure would further undergo either N−H dissociation to form a CA-RA bidentate configuration or O−H dissociation to form a CA-CA bidentate configuration. The higher relative surface concentration observed for the CA-RA configuration than that of the CA-CA configuration therefore suggests that kinetic effects may play an important role in the adsorption of GG on Si(111)7×7, upon consideration of the respective calculated adsorption energies (Figure 2). On the other hand, N−H dissociative adsorption of GG on an AA site would also be followed by either N−H dissociation to form an AA-RA bidentate or O−H dissociation to form an AA-AA bidentate configuration. However, unlike the CA site with two adjacent RA sites, an AA site is adjacent to just one RA site. The formation of an AA-AA bidentate configuration, requiring one RA site each across the dimer wall, is therefore more likely than an AA-RA bidentate configuration, requiring one RA site adjacent to the initial AA site plus two additional RA sites nearby. This accounts for the observation that AA-AA has a higher relative surface concentration than AA-RA. By the same token, CA-RA, with two adjacent RA sites, would have a higher relative surface concentration than AA-RA, with just one RA site. As the exposure increases resulting in more RA sites being occupied by the configurations, the growth of CA-RA (AA-RA) configuration, requiring three RA sites, becomes slower than that of CA-CA (AA-AA), requiring just two RA sites. Furthermore, the number of RA sites per unit cell is half of the total number of adatoms (CA+AA), the reduced availability of RA sites would have a larger effect on the growth of the CA-RA (AA-RA) than that of CA-CA (AA-AA). These effects contribute to the observed slower increase with increasing exposure for CA-RA than that for CA-CA. Finally, the CA-AA configuration has the lowest relative surface concentration over all the exposures, suggesting that the larger CA-to-AA separation (7.68 Å) is least favorable for bidentate adsorption, possibly due to steric effects.

We also show in Figure 3f the total CA and AA relative occupancies as well as the total coverage. The total CA (AA) site occupancy is given by the sum of the relative surface concentration of CA-RA (AA-RA) and that of CA-AA plus twice the relative surface concentration of CA-CA (AA-AA), while the total coverage (or total adatom occupancy) corresponds to the sum of CA and AA relative occupancies. Evidently, the higher total CA occupancy is nearly the same as the total AA occupancy over the entire exposure range. This indicates that there is minimal surface diffusion upon GG impact onto the surface and the adsorption appears to be purely statistical, despite the higher reactivity of the CA site than the AA site expected for other small organic molecules. The process of forming a bidentate configuration is therefore rapid, and the two resulting bonds are apparently strong enough to prevent surface diffusion of the adsorbate. In addition, the total coverage of GG is found to increase near-linearly from 3.4% for 15 s exposure to 7.5% for 40 s exposure. Adsorption involving bidentate configurations on two Si sites for GG is statistically less favorable than the unidentate adsorption on a single Si site as in the glycine case, which could account for the difference in the amount of adsorption. Finally, the free −CONH− and −COOH groups remaining on the respective bidentate adstructures offer viable sites to facilitate adsorption of a second adlayer through the formation of hydrogen bonding. Such type of H-bond mediated growth process has been observed in our recent XPS work.[20] However, in contrast to the unidentate adsorption structures of glycine, the geometries imposed by the bidentate adsorption structures are expected to be less flexible for such type of H-bonding formation.

4. CONCLUSION

The early adsorption process of glycylglycine on Si(111)7×7 at room temperature is studied by direct STM imaging and DFT calculations. The present work not only confirms our recent XPS results which suggest that adsorption of GG involves either N−H and O−H dissociation or double N−H dissociation, but also directly identifies five general types of site-specific bidentate bonding arrangements on the 7×7 surface. Using filled-state STM imaging, we are able to demonstrate that N−H and O−H dissociation occurs on an adatom−adatom pair across or on the same side of a dimer wall while double N−H dissociation occurs at an adatom−restatom pair. More importantly, our STM results show that both types of double dissociation on specific Si sites are equally probable. We further determine that the relative surface concentrations of the five bidentate configurations follow the ordering: CA-RA > AA-AA > CA-CA > AA-RA > CA-AA over the exposure range (up to 40 s) used in the present work. Our DFT calculations employing large $Si_{26}H_{24}$ and $Si_{16}H_{18}$ clusters as model surfaces further support that all five bidentate configurations are thermodynamically viable. In addition, the total relative occupancies of the CA and AA sites are found to be essentially the same. These observations point to the pure statistical nature of the adsorption process, suggesting that the adsorption essentially occurs at the random points of molecular impact and the bidentate interactions are sufficiently strong to prevent surface diffusion. The present work shows that STM investigation in combination with XPS/DFT studies offers a powerful site-specific analysis of the surface adsorption of these interesting multifunctional molecules.

AUTHOR INFORMATION

Corresponding Author

*E-mail: tong@uwaterloo.ca.

Notes

The authors declare no competing financial interest.

ACKNOWLEDGMENTS

The present work was supported by the Natural Sciences and Engineering Research Council of Canada.

REFERENCES

(1) Hamers, R. J. *Annu. Rev. Anal. Chem.* **2008**, *1*, 707−36.
(2) Allara, D. L. *Biosens. Bioelectron.* **1995**, *10*, 771−783.
(3) Mirkin, C. A.; Ratner, M. A. *Annu. Rev. Phys. Chem.* **1992**, *43*, 719−754.
(4) Aviram, A.; Ratner, M. A. *Chem. Phys. Lett.* **1974**, *29*, 277−283.
(5) Bergveld, P. *Sens. Actuators, A* **1996**, *56*, 65−73.
(6) Wolkow, R. A. *Annu. Rev. Phys. Chem.* **1999**, *50*, 413−441.
(7) Leftwich, T.; Teplyakov, A. *Surf. Sci. Rep.* **2007**, *63*, 1−71.
(8) Radi, A.; Ebrahimi, M.; Leung, K. T. *Surf. Sci.* **2010**, *604*, 1073−1081.
(9) Yoshinobu, J. *Prog. Surf. Sci.* **2004**, *77*, 37−70.
(10) Filler, M. a.; Bent, S. F. *Prog. Surf. Sci.* **2003**, *73*, 1−56.
(11) Takahashi, S.; Takahashi, M.; Tanishiro, Y.; Takayanagi, K. *J. Vac. Sci. Technol., A* **1985**, *3*, 1502−1506.
(12) Tao, F.; Xu, G. Q. *Acc. Chem. Res.* **2004**, *37*, 882−93.
(13) Northrup, J. E. *Phys. Rev. Lett.* **1986**, *57*, 154−157.
(14) Waltenburg, H. N.; Yates, J. T. *Chem. Rev* **1995**, *95*, 1589−1673.

(15) Ebrahimi, M.; Chong, J. M.; Leung, K. T. *J. Phys. Chem. C* **2010**, *114*, 2947−2957.
(16) Ebrahimi, M.; Leung, K. T. *Surf. Sci.* **2009**, *603*, 1203−1211.
(17) Radi, A.; Leung, K. T. *Mater. Express* **2011**, *1*, 144−153.
(18) Qu, Y.; Wang, Y.; Li, J, W.; Han, K.-L. *Surf. Sci.* **2004**, *569*, 12−22.
(19) Huang, J. Y.; Ning, Y. S.; Yong, K. S.; Cai, Y. H.; Tang, H. H.; Shao, Y. X.; Alshahateet, S. F.; Sun, Y. M.; Xu, G. Q. *Langmuir* **2007**, *23*, 6218−26.
(20) Zhang, L.; Chatterjee, A.; Ebrahimi, M.; Leung, K. T. *J. Chem. Phys.* **2009**, *130*, 121103.
(21) Luo, X.; Qian, G.; Sagui, C.; Roland, C. *J. Phys. Chem. C* **2008**, *112*, 2640−2648.
(22) Lopez, A.; Heller, T.; Bitzer, T.; Richardson, N. V. *Chem. Phys.* **2002**, *277*, 1−8.
(23) Zhang, L.; Chatterjee, A.; Leung, K. T. *J. Phys. Chem. C* **2011**, *115*, 14155.
(24) Tabata, H.; T. Kawai, M. K. *Surf. Sci.* **1995**, *342*, 215−223.
(25) Tabata, H; T. Kawai, M. K. *Surf. Sci.* **1996**, *357*−*358*, 195−201.
(26) El Garah, M.; Palmino, F.; Chérioux, F.; Melinte, S.; Hackens, B.; Rodrigues, M.; Bogdan, D.; Duverger, E. *Phys. Rev. B* **2012**, *85*, 2−6.
(27) Chatterjee, A.; Zhang, L.; Leung, K. T. *J. Phys. Chem. C* **2012**, *116*, 10968.
(28) Klein, M.; Schwitzgebel, G. *Rev. Sci. Instrum.* **1997**, *68*, 3099−3103.
(29) *NIST Chemistry WebBook*; http://webbook.nist.gov/chemistry.
(30) Frisch, M. J.; Trucks, G. W.; Schlegel, H. B.; Scuseria, G. E.; Robb, M. A.; Cheeseman, J. R.; Scalmani, G.; Barone, V.; Mennucci, B.; Petersson, G. A.; Nakatsuji, H.; Caricato, M.; Li, X.; Hratchian, H. P.; Izmaylov, A. F.; Peralta, J. A.; Peralta, J. E.; Ogliaro, F.; Bearpark, M.; Heyd, J. J.; Brothers, E.; Kudin, K. N.; Staroverov, V. N.; Kobayashi, R.; Normand, J.; Raghavachari, K.; Rendell, A.; Burant, J. C.; Iyengar, S. S.; Tomasi, J.; Cossi, M. *GAUSSIAN 09*; Gaussian Inc.: Wallingford, CT, 2009.
(31) Becke, A. D. *J. Chem. Phys.* **1993**, *98*, 5648−5652.
(32) Lee, C.; Yang, W.; P., R. G. *Phys. Rev. B* **1988**, *37*, 785−789.
(33) Gil, A.; Bertran, J.; Sodupe, M. *J. Chem. Phys.* **2006**, *124*, 154306.
(34) Chatterjee, A.; Zhang, L.; Leung, K. T. To be published.